Ocean Engineering 266 (2022) 112831

Contents lists available at ScienceDirect

Ocean Engineering

journal homepage: www.elsevier.com/locate/oceaneng

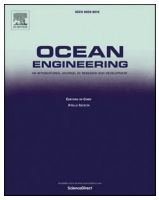

Compressive creep behavior of spherical pressure hull scale model for full-ocean-depth manned submersible

Lei Wang [a,b,c,*], Yanqing Li [a,b,c], Chengqi Sun [d,e], Jianke Qiu [f], Jinhao Huang [a,b,c], Xuyin Jiang [a,b,c], Zhijie Sun [g], Zhengquan Wan [a,b,c]

[a] China Ship Scientific Research Center, Wuxi, 214082, China
[b] State Key Laboratory of Deep-sea Manned Vehicles, Wuxi, 214082, China
[c] Taihu Laboratory of Deepsea Technological Science, Wuxi, 214082, China
[d] State Key Laboratory of Nonlinear Mechanics, Institute of Mechanics, Chinese Academy of Sciences, Beijing, 100190, China
[e] School of Engineering Science, University of Chinese Academy of Sciences, Beijing, 100049, China
[f] Institute of Metal Research, Chinese Academy of Sciences, Shenyang, 110016, China
[g] Luoyang Ship Material Research Institute, Luoyang, 471023, China

ARTICLE INFO

Keywords:
Full-ocean-depth manned submersible
Titanium alloy
Pressure hull
Compressive creep behavior
Creep constitutive equation

ABSTRACT

The phenomenon of room temperature creep in titanium alloys has drawn great attention for decades. With the increasing application of titanium alloys to the manned submersible pressure hull, the traditional calculation and analysis based on strength and stability cannot meet the requirement of structure design and safety evaluation for the spherical pressure hull completely. In this paper, a series of compressive creep tests were performed to reveal the change rule and distribution characteristics for creep behavior of the spherical pressure hull model. Results show that there is no measurable creep strain for pressure hull under maximum operating pressure and steady-state creep appeared in high stress areas of the pressure hull under 1.25 times maximum operating pressure, with the characteristics of internal creep strain and strain rate being greater than the external counterparts. The stress threshold value of the pressure hull model for steady-state creep is 853.7 MPa (equivalent to $0.88R_{p0.2}$), and a creep constitutive equation is proposed based on improved Norton power law model. The results of this paper can provide support for the safety assessment and optimization design of manned submersibles for long-term service.

1. Introduction

Titanium alloys have become the most promising engineering materials used in deep-sea vehicles such as pressure hulls of manned submersibles (Wang and Cui, 2015; Cui, 2013; Takagawa et al., 1995; Pan and Cui, 2012) due to their high strength to weight ratio, low diffusivity, excellent corrosion resistance and satisfactory weldability (Bache, 2003; Ma et al., 2021; Sun et al., 2020; Wang et al., 2020; Xi et al., 2020; Corigliano and Crupi, 2021). Under the trend of manned submersibles' working depth increasing, titanium alloys can satisfy the requirements of lightweight, corrosion resistance and security for deep-sea manned submersibles. However, titanium alloys could suffer from creep problem at room temperature (Ankem et al., 1994; Jaworski and Ankem, 2006; Neeraj et al., 2000; Savage et al., 2002). Different from the creep of airframes and engines in aerospace caused by tensile loads at high temperature (Gudipati and Kosaka, 2011; Kumar et al., 2018; Dong et al., 2018; Kotkunde et al., 2014), the creep of titanium alloys in deep sea environment is induced by compressive loads at about 4 °C, the structure is under high pressure, and local stress could even approach the yield strength.

A significant amount of research has been reported to reveal the compressive creep behavior of titanium alloys at room temperature. The factors which could play important roles on creep behavior, involving chemical composition, microscopic structure, stress level, creep time, stress state and so on, have been investigated in the open literatures (Ankem et al., 2013; Barboza et al., 2006; Kassner et al., 2015; Peng et al., 2014; Dai et al., 2015; Kassner and Smith, 2014; Sato et al., 2006). CP-Ti has shown only compressive primary creep at room temperature, and no steady-state creep appears (Peng et al., 2014; J. Zhang et al., 2018). Compressive stress threshold has been found to exist in the

* Corresponding author. China Ship Scientific Research Center, Wuxi, 214082, China.
E-mail address: wanglei@cssrc.com.cn (L. Wang).

https://doi.org/10.1016/j.oceaneng.2022.112831
Received 13 August 2022; Received in revised form 23 September 2022; Accepted 5 October 2022
Available online 21 October 2022

compressive creep tests of titanium alloys. When the compressive stress value reaches the steady-state creep threshold, the creep strain will increase linearly (Yu et al., 2020; Wang et al., 2018). It has been shown that both power law and logarithmic constitutive models considering the influence factors such as creep stress, creep time and creep strain rate can describe the creep behavior of titanium alloys well in various conditions, while the fitness of exponential law constitutive model and sine law constitutive model is poor at ambient temperature (Harrison et al., 2013; Yang and Ling, 2017; Gray and Whittaker, 2015).

The spherical pressure hull fabricated from titanium alloys provides a safe space for pilots and scientists, which is the critical component of manned submersibles. Structural strength and stability are traditionally analyzed for the safety evaluation and design calculation of pressure structures (Pan and Cui, 2010; M.Y. Zhang et al., 2018; Yu et al., 2022), however, very few creep behavior of pressure hull were reported in the research of deep submersibles during long-term service. The Alvin submersible has completed upgrades of manned cabin fabricated from Ti–6Al–4V ELI (extra-low interstitial), and the new manned spherical hull is capable of a maximum operating depth of 6500 m in sea water with no creep (Boyer and Williams, 2011). For the titanium alloy spherical hull of full-ocean-depth manned submersible, a critical problem of structure safety evaluation for long-term service is whether or not the creep occurs. The distribution characteristics and variation laws for creep of titanium alloy hull remain unclear, and it is necessary to conduct creep test for manned spherical hull in the absence of practical experience.

In order to reveal the compressive creep behavior of pressure hull of full-ocean-depth manned submersibles, high-pressure creep tests are performed systematically on a spherical pressure hull scale model in this paper, and strains of typical measurement points on the internal and external surface of the scale model are obtained. Moreover, the compressive stress threshold for primary creep of the pressure hull scale model is presented based on structural stress analysis. At last, a compressive creep constitutive equation considering stress threshold of steady-state creep is developed.

2. Materials and methods

2.1. Materials

The pressure hull scale model for full-ocean-depth manned submersibles was fabricated by a high strength titanium alloy Ti–6Al–2Sn–2Zr–3Mo-X. The microstructure of the material is bimodal microstructure consisting of primary α phase and transformed β as shown in Fig. 1. The volume percentage of primary α phase is about 16.63%.

2.2. Pressure hull scale model

The pressure hull scale model is designed according to the full-size pressure hull of full-ocean-depth manned submersible, and assembled by the spherical hull, access hatch and hatch cover, as shown in Fig. 2. Main parameters of the pressure hull scale model are shown in Table 1.

The pressure hull scale model was fabricated by the processing technologies containing hemisphere integral stamping forming, precision machining, vacuum electron beam welding, bulk heat treatment. Both of sheets and forgings were used for the construction materials. Sheets were stamped to two hemispherical hulls, and forgings were processed precisely to the access hatch and hatch cover. Both ends of the upper hemispherical hull with trepanning were welded with lower hemispherical hull and the hatch by vacuum electron beam welding, respectively. The access hatch was connected with the hatch cover by screws and sealed with a nitrile O-ring. Requirements of dimensional control and nondestructive testing were eventually met by inspections after the model processing was completed.

Mechanical property tests of furnace pieces during model fabricating were conducted. Tension and compression specimens were taken from furnace pieces in the surface and core position along the transverse and longitudinal direction, respectively. Mechanical property test results are shown in Table 2.

In Table 2, $R_{p0.2}$ is the proof strength that the non-proportional extension is 0.2%, R_m is tensile strength, E denotes the modulus of elasticity, μ denotes Poisson's ratio, $R_{pc0.2}$ is the proof strength that the non-proportional compressive strain is 0.2%, and E_c is compressive modulus of elasticity.

It should be noted that the Poisson's ratio test results are different from 0.28–0.38. The degree of deformation in the surface and core position of titanium alloy thick plates is not consistent during the rolling process, which leads to a decrease of orientation distribution function for the texture in the thickness direction. Therefore, the influence of texture on mechanical properties of the material decreases, and the mechanical properties of furnace pieces in the surface and core position, including Poisson's ratio, are different.

2.3. Creep testing system

The creep testing system is a large ultra-high pressure testing facility intended for deep-sea environment simulation developed by prestressed steel wire wound technology, as shown in Fig. 3. The test facility is composed of hydraulic pressure tank, preload frame, automatic loading and unloading system, data acquisition system, electrical control system, and safety protection system. It has the characteristics of small working stress amplitude, strong bearing capacity, high fatigue resistance and compact structure. The pressure tank provides a compressive creep test environment under ultra-high pressure for the pressure hull

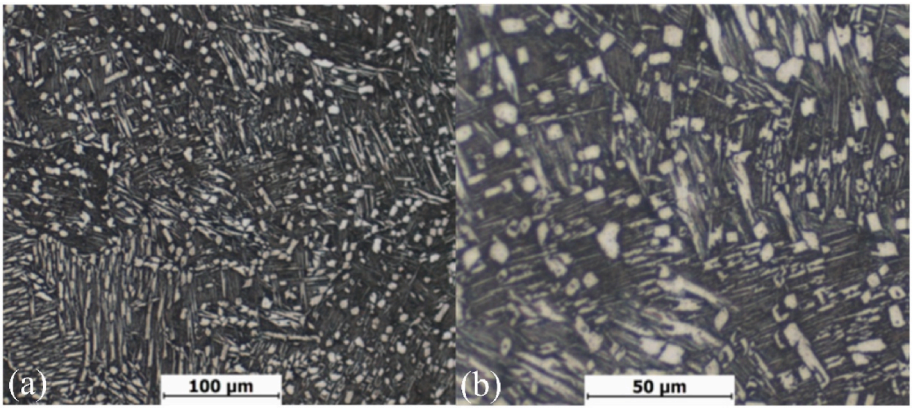

Fig. 1. Optical microstructure and phase composition of the as-received Ti–6Al–2Sn–2Zr–3Mo-X alloy: (a) 100 μm, (b) 50 μm.

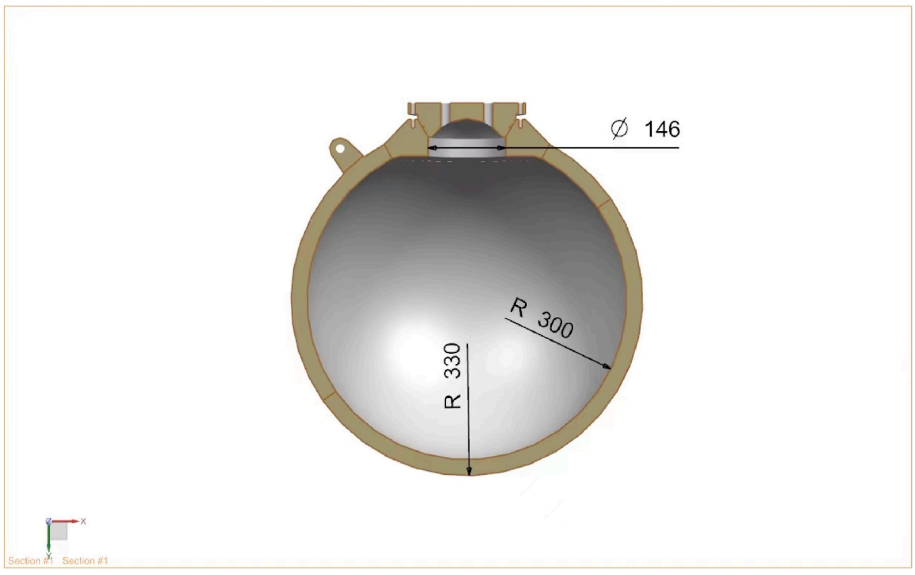

Fig. 2. Schematic of pressure hull scale model in the creep test.

Table 1
Main parameters of the pressure hull scale model.

Inner diameter of spherical hull (mm)	Wall thickness of spherical hull (mm)	Transmission diameter of access hatch (mm)	Total weight (kg)
600	30	146	180

model, with a maximum operating pressure of 200 MPa and an inner diameter of 1600 mm.

The creep test data acquisition system utilizes electrometric method to measure strains, which contains statical strainometer, data processing analyzer, strain gauges, and pressure sensors. The resistance variation signal of strain gauges generated by structural deformation is passed to the strain indicator through wires, which amplifies the output voltage signal of bridge and converts it into strain data. Finally, the strain data is

Table 2
Mechanical properties of furnace pieces.

Tensile tests					Compression tests		
No. of specimens	$R_{p0.2}$ (MPa)	R_m (MPa)	E (GPa)	μ	No. of specimens	$R_{pc0.2}$ (MPa)	E_c (GPa)
T-L-S	969	1108	118	0.36	C-L-S	990	119
T-L-S	960	1103	111	0.37	C-L-S	935	110
T-L-C	970	1129	109	0.28	C-L-C	1025	119
T-L-C	982	1125	110	0.28	C-L-C	1028	122
T-T-S	962	1078	111	0.34	C-T-S	990	112
T-T-S	955	1094	114	0.35	C-T-S	1014	116
T-T-C	970	1087	111	0.33	C-T-C	1023	120
T-T-C	959	1078	110	0.38	C-T-C	1026	117
Average	966	1100	112	0.34	Average	1004	117

Fig. 3. Creep testing system.

processed by the data processor and displayed in real time.

2.4. Creep testing procedure

2.4.1. Measuring points

According to creep behavior laws of titanium alloy materials, stress level is an essential factor affecting creep. Therefore, we suppose that the structure is prone to creep in locations with higher stresses. In order to measure structural creep strain, strain gauges are usually arranged in high stress areas such as the positions near welds. To reveal the stress state of the model integrally, strain gauges were arranged on both the internal and external surface of the spherical hull model, numbered sequentially with A and E as the first letters, respectively.

Representative positions of the pressure hull model were selected to paste the bidirectional strain gauges, including typical spherical hull, two sides of hemispherical butt weld, two sides of hatch weld, and the positions of the minimum thickness of the upper and lower hemispherical hull, as shown in Fig. 4. The two directions of the strain gauge follow the longitude and latitude of the spherical hull, respectively.

Temperature compensated testing plates, which are of the same material as the pressure hull scale model, were utilized to minimize the effect of changes in temperature. The compensation plates were pasted with strain gauges and placed into the pressure tank together with the model. The number of strain gauges for the pressure hull model are shown in Table 3.

2.4.2. Test preparation

Strain measurement preparations were carried out according to the strain gauge layout plan, involving point positioning, surface grinding, pasting strain gauges, connecting with wires and sealing, as shown in Fig. 5.

The wires inside the model are exported from the model via watertight connectors on the hatch cover, while the wires outside of the model are exported from the pressure tank via watertight connectors on the upper end cover of the pressure tank. In this way, strain data from the internal and external measurement points of the model are transmitted to the data processing analyzer.

After the model lifting and pipeline assembling, the test preparation work is accomplished.

2.4.3. Test pressure

The maximum operating depth of the full-ocean-depth manned submersible is 11,000 m, and the density of seawater is 1025.26 kg/m^3 on average based on statistics. Therefore, the hydrostatic pressure corresponding to the maximum operating depth is 110.52 MPa. According to the rules for submersibles (CCS, 2018), the maximum operating pressure is determined according to the maximum operating depth and the specified ultra-deep depth. Considering that the ultra-depth value is not less than 50 m, the maximum operating pressure was finally determined to be 115 MPa.

In this paper, three hydrostatic pressures were selected: maximum operating pressure of 115 MPa, 1.13 times maximum operating pressure of 130 MPa, and 1.25 times maximum operating pressure of 144 MPa.

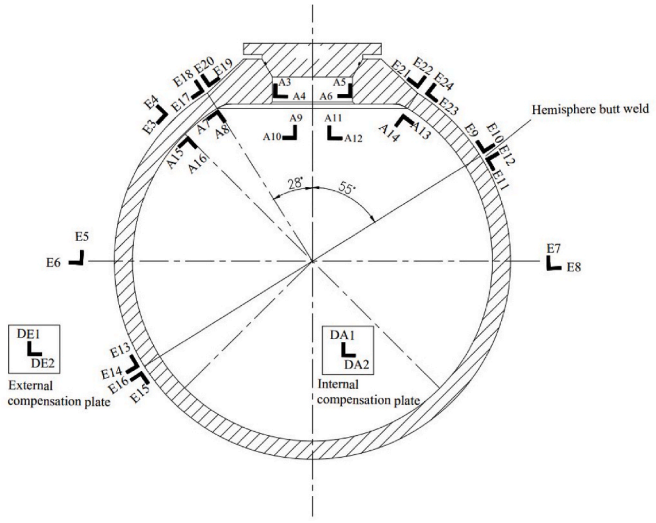

Fig. 4. Schematic of strain gauge arrangement.

Table 3
Number of strain gauges for the pressure hull scale model.

Measuring point location	Number of measuring points	Number of strain gauges	Internal/ external	No.
Temperature compensated testing plates	2	4	External	(DE1, DE2)
			Internal	(DA1, DA2)
Spherical hull	6	12	External	(E03, E04) (E05, E06) (E07, E08)
			Internal	(A09, A10) (A11, A12) (A15, A16)
Hemispherical butt weld	4	8	External	(E09, E10) (E11, E12) (E13, E14) (E15, E16)
Hatch weld	6	12	External	(E17, E18) (E19, E20) (E21, E22) (E23, E24)
			Internal	(A07, A08) (A13, A14)
Inner wall of the hatch	2	4	Internal	(A03, A04) (A05, A06)
Minimum thickness of the spherical hull	2	4	External	(E25, E26) (E27, E28)

2.4.4. Test procedure

Fig. 7 shows the loading history of the creep test. Firstly, the pressure of 60 MPa is preloaded to the model in order to check whether the model is leaking and whether the facilities are working properly. Then, the pressure is increased to 115 MPa to obtain the strain data of measuring points. Several factors are considered comprehensively to determine the load dwell time, including the maximum working time of a single voyage for the full-ocean-depth submersible, the number of dives for each voyage, the safety factor for the calculation of structural stability, and the safety assessment of long-term service. Finally, creep tests under the hydrostatic pressure of 115 MPa, 130 MPa and 144 MPa are performed as shown in Fig. 6. The pressure triggering function of data acquisition system is utilized to extract the strain value more accurately

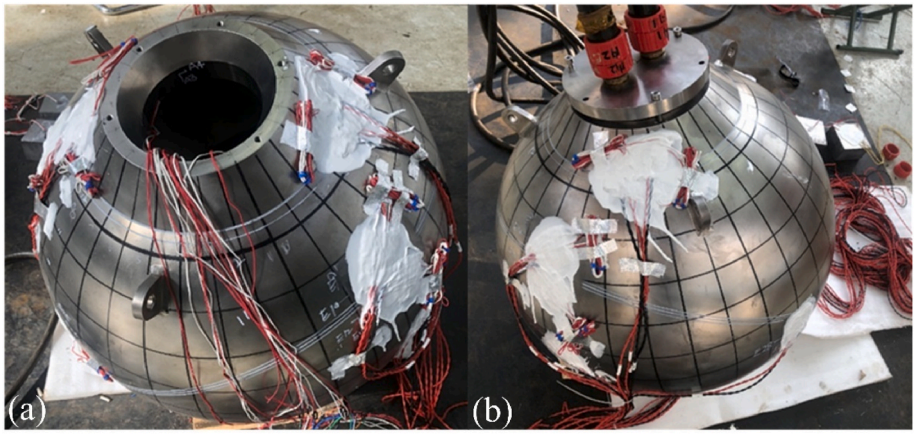

Fig. 5. Test preparations: (a) strain gauges pasted outside the model, (b) the model and watertight connectors on the hatch cover.

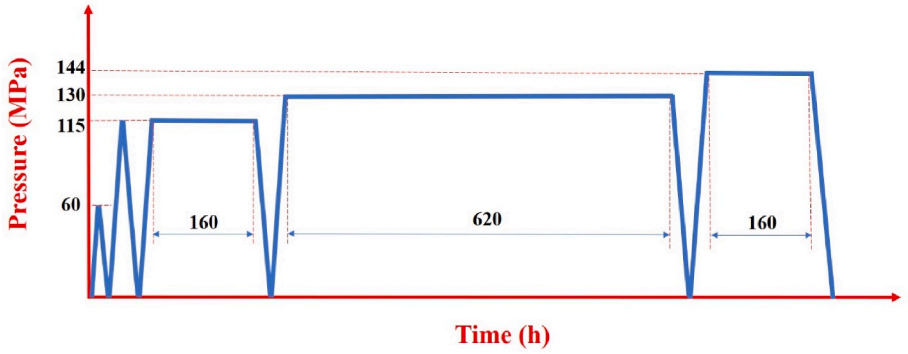

Fig. 6. Schematic of loading history in the whole test.

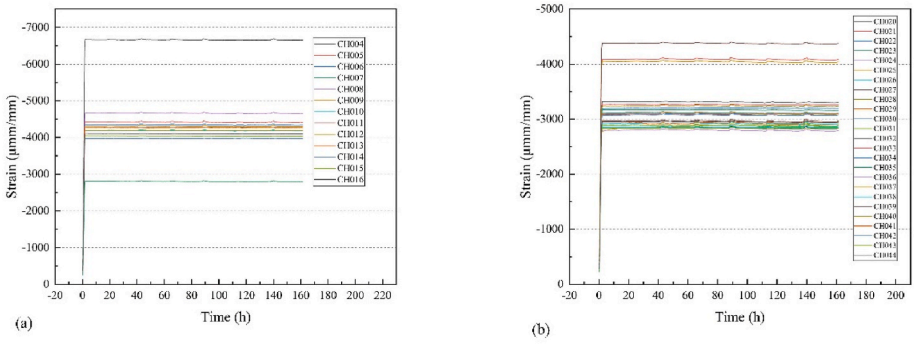

Fig. 7. Strain-time curves of measuring points on the internal and external surface of the model under 115 MPa: (a) internal, (b) external.

at the specified pressure to minimize the effect of small pressure fluctuations during creep tests.

3. Results and discussions

3.1. Test results

3.1.1. Results under the pressure of 115 MPa

According to the test procedure, after the pressure had reached the pressure of 115 MPa, the creep test was started under constant pressure with the continuous dwell time of 160 h. The strain data of measuring points on the internal and external surface of the model is derived, and the corresponding strain-time curves are plotted as shown in Fig. 7.

It is seen from the strain curves in Fig. 7 that after the applied pressure reaches 115 MPa, the strain of each measuring point remains unchanged except for the system drifts.

3.1.2. Results under the pressure of 130 MPa

After the dwell time of 160 h under the pressure of 115 MPa, the target pressure was raised to 130 MPa for the creep test with the dwell time of 620 h. The strain-time curves under the pressure of 130 MPa are shown in Fig. 8.

As is seen from Fig. 8, at the constant pressure of 130 MPa, the measuring points inside and outside the pressure hull model do not show increasing strains over time, namely, there is no creep strain occurrence in the pressure hull scale model under the pressure of 130 MPa.

3.1.3. Results under the pressure of 144 MPa

According to the test procedure in Fig. 6, the test pressure was lastly increased to 144 MPa, and the dwell time was 160 h. Here, the strain

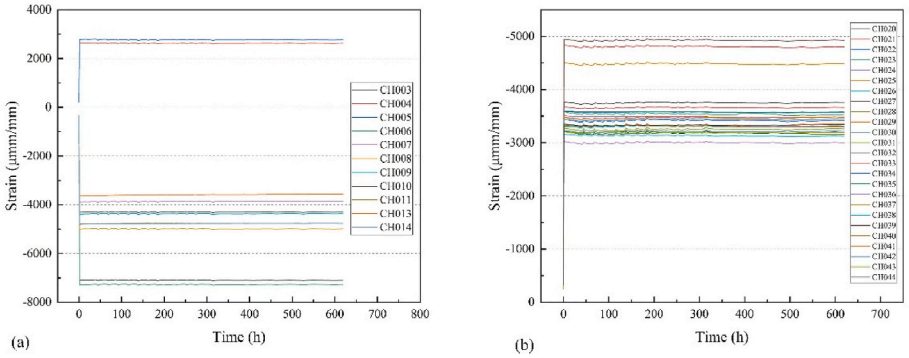

Fig. 8. Strain-time curves of measuring points on the internal and external surface of the model under 130 MPa: (a) internal, (b) external.

data during the loading process was derived.

Under the combined action of ultra-high hydrostatic pressure and long dwell time, some gauges were detached from the pressure hull, resulting in data exception. Therefore, gauges that show abnormal behavior should not be used to investigate for creep, and the strain-pressure curves were plotted based on valid data, shown in Fig. 9.

It is seen from the curves that strains during the loading process vary linearly with the increase of pressure. Therefore, the structure is in an elastic state, and there is no plastic deformation during the loading process.

The strain-time curves of the internal and external measuring points under the constant pressure of 144 MPa are shown in Fig. 10.

According to Fig. 10, the creep curves under the constant pressure of 144 MPa can be divided into two typical stages. The first stage is the primary creep, in which the creep strain rate decreases gradually with loading time. The second stage is the steady-state creep, where the creep strain rate tends to be a constant value. The curves do not have tertiary creep stage with increasing loading time. During the primary creep, the compressive creep strain that increase with loading time by power law occurs at most of the measuring points on the internal and external surface of the pressure hull scale model.

For the measuring points on the external surface of the spherical hull model, the creep strain that increases in the first stage of the creep curve does not continue to grow in the secondary stage, the creep strain rate of the secondary stage eventually tends to be zero and no longer changes. The creep strains at different positions outside the model under the pressure of 144 MPa are shown in Table 4. The measuring point on the external surface of the model corresponding to the maximum creep strain value is located near the circumferential hatch weld, which is the high stress zone of the model, with the strain gauge number of E17 and the cumulative creep strain of −148 με. Two measurement points near the hatch weld present a steady-state creep in which the creep strain increases with loading time. There is a large strain change near the hemisphere butt weld, and the cumulative creep strain of the measuring point E9 was −120 με. Due to the differences in position and thickness of the measuring points, the creep strain at the typical position of the spherical hull shows a certain range of dispersion, and the creep strain at the minimum thickness position of the spherical hull is −113 με.

For the measuring points on the internal surface of the spherical hull model, the measured creep strains under the pressure of 144 MPa are shown in Table 5. The A3, A6, A8, A9, and A10 measuring points located inside the spherical hull present the steady-state creep. For the above measuring points, when the stress of the measuring point is smaller, the creep strain and creep strain rate are lower, and the time of the primary creep is longer. The measuring point on the internal surface of the model corresponding to the maximum creep strain value is located on the internal surface of the hatch cylindrical section, with the strain gauge number of A3 and the cumulative creep strain of −147 με. The measuring point corresponding to the extreme stress of the spherical hull model is located on the internal surface of the hatch cylindrical section, the circumferential direction of which presents the extreme point of the creep strain. The longitudinal stress along the hatch cylindrical section is the tensile stress, under which the strain gauge A4 is to obtain a tensile creep strain of 110 με. The creep strains at the position of typical spherical hull plate inside the model are small, the variation range of which is −31 με to −79 με.

3.2. Stress analysis

In order to further understanding the stress state of the spherical pressure hull scale model under hydrostatic pressure, the stress analysis is performed according to the Lamé formulae, finite element method and the method based on test data.

3.2.1. Stress calculation methods

(1) Lamé formulae

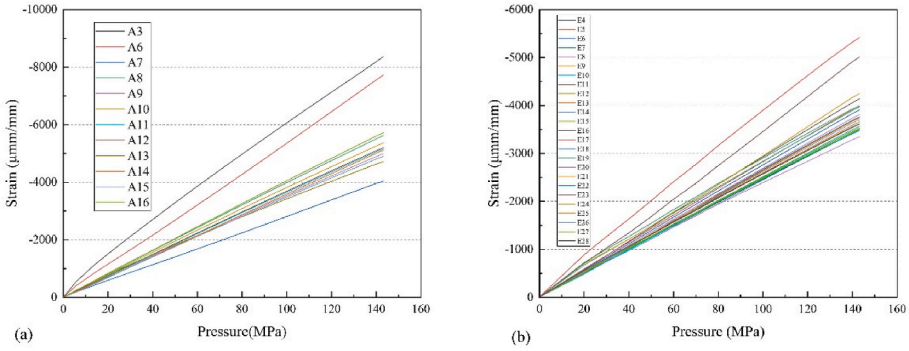

Fig. 9. Strain-pressure curves with specified pressure of 144 MPa during the loading process: (a) internal, (b) external.

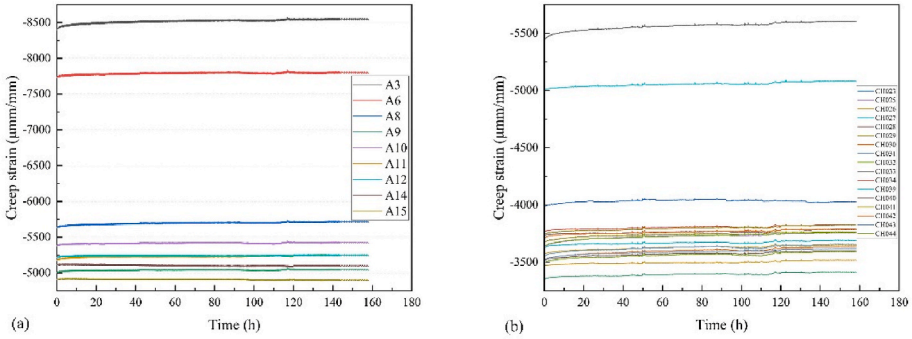

Fig. 10. Strain-time curves under constant pressure of 144 MPa: (a) internal, (b) external.

Table 4
Creep strains of the measuring points on the external surface of the spherical hull model.

Location	Hatch weld			Hemispherical butt weld				Spherical hull plate	
No.	E17	E20	E23	E9	E14	E15	E26	E27	E28
Creep strain (με)	−148	−54	−67	−120	−109	−95	−72	−91	−113

Table 5
Creep strains of the measuring points on the internal surface of the scale model.

No.	A3	A4	A5	A6	A8	A9	A10	A11	A12
Creep strain (με)	−147	110	52	−57	−79	−37	−38	−69	−31

The spherical pressure hull model in this paper is regarded as a medium-thickness-walled hull due to thickness-radius ratio. According to the results in Fig. 10, the structure is in an elastic state.

The solution of stress problem of the medium-thickness-walled spherical hull structure in the elastic state can be traced back to the work by Lamé (1852). Exact solutions for the maximum principal stress of the thick-walled spherical hull under uniform pressure are as follows according to the Lamé formulae:

$$\left.\begin{aligned}\sigma_r &= \frac{R_i^3 p_i}{R_o^3 - R_i^3}\left(1 - \frac{R_o^3}{r^3}\right) - \frac{R_o^3 p_o}{R_o^3 - R_i^3}\left(1 - \frac{R_i^3}{r^3}\right)\\ \sigma_\theta &= \frac{R_i^3 p_i}{R_o^3 - R_i^3}\left(1 + \frac{R_o^3}{2r^3}\right) - \frac{R_o^3 p_o}{R_o^3 - R_i^3}\left(1 + \frac{R_i^3}{2r^3}\right)\end{aligned}\right\} \quad (1)$$

where σ_r is the radial stress, σ_θ is the circumferential stress, R_i is the inner radius of the spherical hull, R_o is the outer radius of the spherical hull, p_i is the internal pressure, and p_o is the external pressure.

Substituting the model dimensions into equation (1), the circumferential stress of −862.2 MPa on the internal surface, −790.2 MPa on the external surface, and −822.5 MPa in the middle surface of the spherical model are obtained.

(2) *Finite element method*

A finite element analysis model is established according to the pressure hull dimensions, and the finite element mesh is partially refined at the position of access hatch.

Load conditions: a 144 MPa load is applied to the external surface of the model, which is converted to the corresponding equivalent load at the cone surface of the hatch. Boundary conditions: three points are selected on the spherical hull for constraints, and each point is constrained by 2 displacement components. The setting of symmetry boundary conditions not only eliminates the rigid body displacement of the entire structure, but also does not restrict the relative deformation [36].

Continuous contours of von Mises stress of the spherical hull model are shown in Fig. 11. Fig. 12 shows the profile at the typical location of spherical hull plate and the circumferential stresses on the inner, middle, and outer surfaces. The circumferential stresses on the inner surface, outer surface and middle surface are −868.5 MPa, −794.0 MPa, and −828.0 MPa, respectively.

(3) Method based on test data

In this method, the spherical coordinates ρ, θ, φ are introduced with the origin at the center of the sphere, and the radial stress is ignored. In this case, it is equivalent to a state of biaxial stress. Circumferential stresses of the spherical hull model are calculated according to Eq. (2):

$$\sigma_\theta = \frac{E}{1-\mu^2}(\varepsilon_\theta + \mu\varepsilon_\varphi)\sigma_\varphi = \frac{E}{1-\mu^2}(\varepsilon_\varphi + \mu\varepsilon_\theta) \quad (2)$$

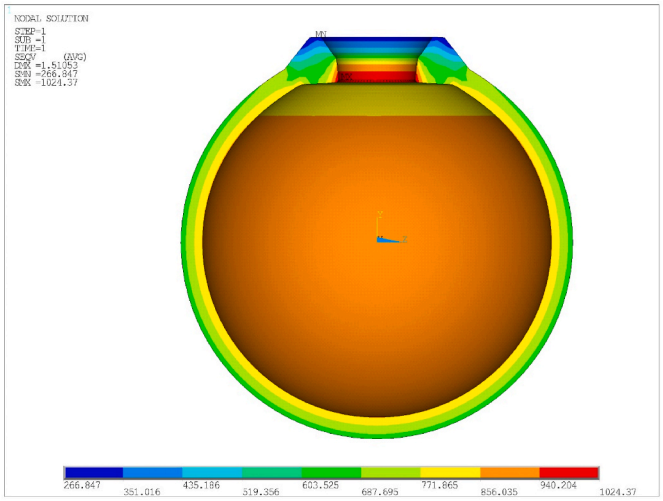

Fig. 11. Continuous contours of von Mises stress of the spherical hull model.

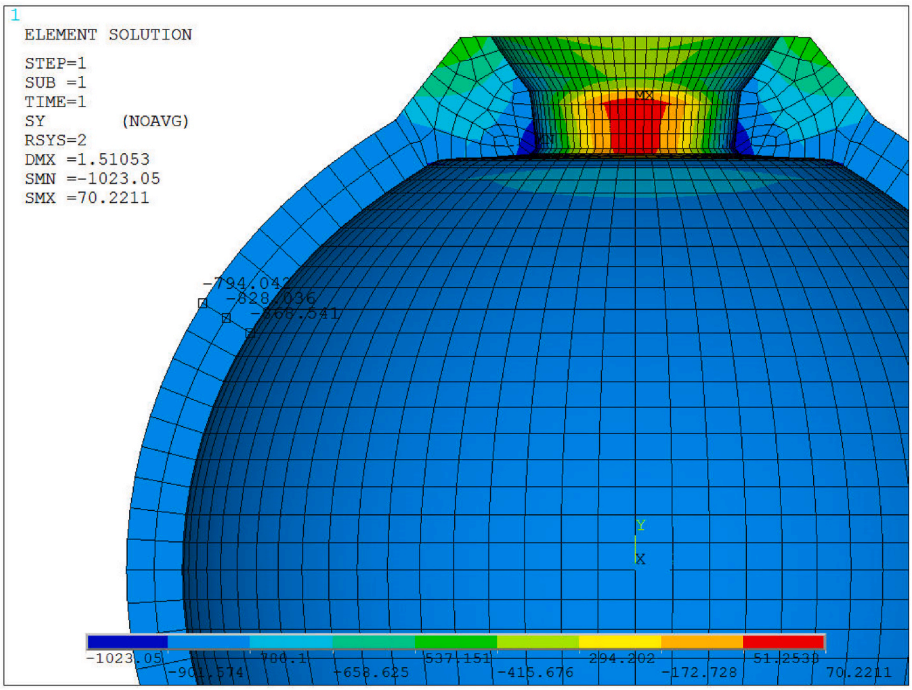

Fig. 12. Stress analysis of the spherical hull model under the pressure of 144 MPa.

where σ_θ and ε_θ are the θ-coordinate stress and strain, σ_φ and ε_φ are the φ-coordinate stress and strain.

The creep test in this paper is a hydrostatic pressure test for simulating the deep-sea ultra-high external pressure environment, and all of the three tested pressures are not less than the maximum operating pressure of the full-ocean-depth manned submersible. Therefore, the pressure effect needs to be considered. The pressure effect of the strain gauge in the hydrostatic pressure environment refers to the phenomenon that the strain gauge deformation due to the hydrostatic pressure will lead to the error of structural strain measurement.

The additional strain caused by the deformation of compensation plates under hydrostatic pressure can be calculated according to the generalized Hooke law:

$$\varepsilon_c = \frac{-1+2\mu}{E} P \tag{3}$$

where ε_C denotes compensation strain, and P is the hydrostatic pressure in the creep test.

According to the method of strain measurement using the compensated plate, the correction between the measured strain ε_A displayed on the instrument and the true strain ε is corrected by:

$$\varepsilon = \varepsilon_A + \varepsilon_c \tag{4}$$

Substitution of the corrected true strains into Eq. (2), the circumferential stresses on the external surface are obtained for the spherical hull model.

3.2.2. Stress calculation results

Based on the above three methods, the stresses on the internal, middle and external surface of the typical spherical hull are calculated under the pressure of 130 MPa and 144 MPa, and the results are summarized in Table 6.

As is shown in Table 6, the stresses calculated by the finite element method are in good agreement with the results based on Lamé formulae and the test data.

From the creep testing data under the pressure of 130 MPa in Fig. 8 and the values of circumferential stress calculated in Table 6, it is found that no creep strain occurs at all the measuring points of the model when the structural stress of the spherical hull is less than 784.1 MPa. Therefore, the stress threshold value for the primary creep of the spherical hull model is greater than 784.1 MPa, which is $0.81R_{p0.2}$ compared with the yield strength and $0.78R_{pc0.2}$ compared with the compressive yield strength of the material for the pressure hull model.

3.2.3. Stress equivalence between scale model and actual structure

For comparison, the structural stress is carried out for both the scale model and the pressure hull of the full-ocean-depth manned submersible. The von Mises stresses calculated based on the finite element method under the hydrostatic pressure of 115 MPa are 827 MPa and 832 MPa, respectively, and the stress distribution contours of the hemisphere structure are shown in Fig. 13. The deviation of 0.6% between two stresses can be neglected and it is seen that the stress state of the scale model is equivalent to the counterpart of the pressure hull in the full-ocean-depth manned submersible. Moreover, the main construction technologies of the scale model are identified with that of the full-size

Table 6
Circumferential stresses at typical spherical hull plates based on different calculation methods.

Applied pressure	130 MPa			144 MPa		
Position	Internal surface (MPa)	Middle surface (MPa)	External surface (MPa)	Internal surface (MPa)	Middle surface (MPa)	External surface (MPa)
Lamé formulae	−778.4	−742.7	−713.4	−862.2	−822.7	−790.2
Finite element method	−784.1	−747.5	−716.8	−868.5	−828.0	−794.0
Method based on test data	−790.6	−753.0	−715.3	−873.9	−835.1	−796.2

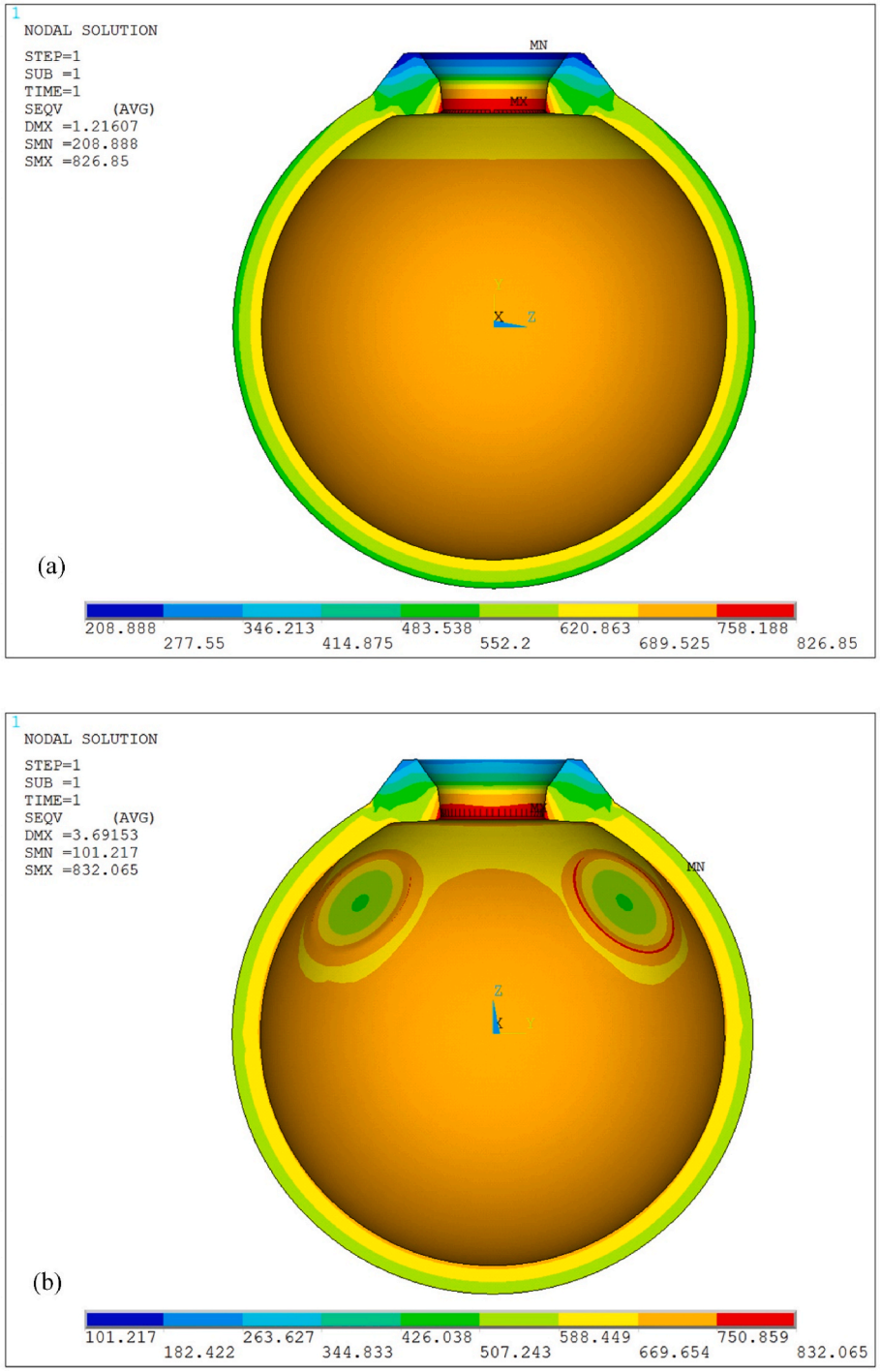

Fig. 13. Stress distribution contours under the hydrostatic pressure of 115 MPa: (a) the scale model, (b) the full-size pressure hull.

pressure hull, and principal dimensions of the scale model are designed according to the scale ratio. This indicates that the result of the scale model in the creep test could represent that of the full-size pressure hull structure, that is, there is no measurable creep in the full-ocean-depth manned submersible under the maximum operating pressure.

3.3. Creep constitutive equation

It is found from the creep curves in Fig. 10 that the creep strain rate gradually decreases and eventually tends to zero at the measuring points outside the model under low stress. While at the measuring points inside the model under high stress, the creep strain gradually enters to the steady-state creep stage with a constant strain rate. This indicates that there is a threshold stress σ_0 for the compressive creep characteristic of the pressure hull scale model of the full-ocean-depth manned submersible. When the stress is greater than σ_0, the creep will enter to the steady-state stage. Otherwise, the creep will saturate, i.e., the creep strain no longer grows. This phenomenon is similar to that of compressive creep characteristic of titanium alloy materials at room temperature [31].

In order to study the relationship between steady creep strain rate and structural stress, the strain data of measuring points which increase linearly are selected, and the creep strain rates for the steady-state creep are calculated, as shown in Table 7.

Norton's equation is modified by introducing the stress threshold

Table 7
Creep strain rate and stress of typical measuring points.

Strain gauge number	A3	A6	A8	A9	A10
Stress (MPa)	−960.3	−892.8	−873.3	−854.9	−864.9
Creep strain rate (h^{-1})	−0.407	−0.316	−0.224	−0.0864	−0.166

σ_0 [20], and a more reasonable relational expression between creep strain rate $\dot{\varepsilon}_s$ and critical stress is expressed as follows:

$$\dot{\varepsilon}_s = A(\sigma - \sigma_0)^m \tag{5}$$

where $\dot{\varepsilon}_s$ is creep strain rate, A denotes a constant related to the material, σ_0 is the stress threshold, and m denotes the creep stress index.

Nonlinear regression analysis of the creep strain rate and stress data are carried out, and the results are illustrated in Fig. 14. The parameters for the creep constitutive equation are listed in Table 8.

As a result, the compressive creep constitutive equation of the titanium alloy pressure hull is present as:

$$\dot{\varepsilon}_s = -0.7753(\sigma - 853.7)^{0.3597} \tag{6}$$

It is seen from Eq. (6) that the compression creep stress threshold value for steady-state creep of the pressure hull model is 853.7 MPa, which is $0.88R_{p0.2}$ compared with the yield strength and is $0.84R_{pc0.2}$ compared with the compressive yield strength of the material for the pressure hull model.

4. Conclusions

In this paper, a new compressive creep test method for titanium alloy pressure hulls of manned submersible was established, and creep tests of the titanium alloy pressure hull model of a full-ocean-depth manned submersible under a series of hydrostatic pressures were performed based on this test method. The main findings of the paper are as follows:

1) It is verified that there is no measurable creep strain for pressure hull scale model of the full-ocean-depth manned submersible under the pressure of 115 MPa and 130 MPa. Since the spherical scale model can represent the full-size pressure hull, it can be indicated that there is no measurable creep occurred in the full-ocean-depth manned submersible under maximum operating pressure.
2) Compressive creep strain occurs at most of the measurement points inside and outside the model under the pressure of 144 MPa, and the steady-state creep even appeared in high stress areas. The creep strain of the spherical hull structure generally presents the distribution characteristics of internal creep strain and strain rate being greater than the external counterparts, and the maximum value of creep strain is located on the internal surface of the access hatch.
3) When the structural stress of the manned spherical hull is less than 784.1 MPa (equivalent to $0.81R_{p0.2}$), no creep strain will occur. The stress threshold value of the pressure hull model for steady-state creep is 853.7 MPa (equivalent to $0.88R_{p0.2}$), and a creep constitutive equation is proposed based on the improved Norton power law model.

The results of this paper can provide support for the safety assessment and optimization design of manned submersibles for long-term service.

CRediT authorship contribution statement

Lei Wang: Methodology, Investigation, Data curation, Formal analysis, Writing – original draft, Writing – review & editing. **Yanqing Li:** Funding acquisition, Formal analysis, Investigation. **Chengqi Sun:** Investigation, Writing – review & editing. **Jianke Qiu:** Methodology, Investigation. **Jinhao Huang:** Investigation, Supervision, Validation.

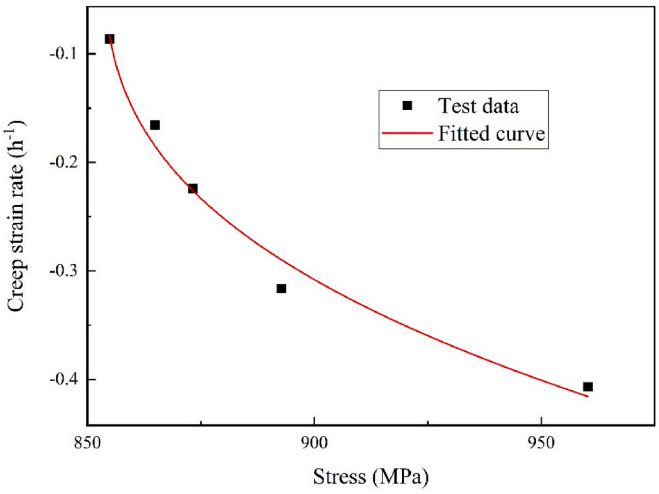

Fig. 14. Regression analysis of the creep strain rate and stress data.

Table 8
Parameters fitted for Eq. (5) using the data from the spherical hull model.

Parameter	A	σ_0	m
Value	−0.07753	853.7	0.3597

Zhengquan Wan: Funding acquisition, Supervision, Validation.

Declaration of competing interest

The authors declare that they have no known competing financial interests or personal relationships that could have appeared to influence the work reported in this paper.

Data availability

Data will be made available on request.

Acknowledgements

The authors gratefully acknowledge the supports of the National Key Research and Development Program of China (No. 2017YFC0305500, No. 2021YFC2802300).

References

Ankem, S., Greene, C.A., Singh, S., 1994. Time dependent twinning during ambient temperature creep of α Ti-Mn Alloy. Scripta Metall. Mater. 30, 803–808.
Ankem, S., Wyatt, Z.W., Joost, W., 2013. Advances in low-temperature creep behavior of single and two-phase titanium alloys. Procedia Eng. 55, 10–16.
Bache, M.R., 2003. A review of dwell sensitive fatigue in titanium alloys: the role of microstructure, texture and operating conditions. Int. J. Fatig. 25, 1079–1087.
Barboza, M.J.R., Perez, E.A.C., Medeiros, M.M., Reis, D.A.P., Nono, M.C.A., Neto, F.P., Silva, C.R.M., 2006. Creep behavior of Ti6Al4V and a comparison with titanium matrix composites. Mater. Sci. Eng. 428, 319–326.
Boyer, R.R., Williams, J.J., 2011. Developments in research and applications in the titanium industry in the USA. In: Proceedings of the 12th world conference on titanium, pp. 10–19.
CCS, 2018. Rules for Classification of Diving Systems and Submersibles. China Classification Society, Beijing.
Corigliano, P., Crupi, V., 2021. Fatigue analysis of TI6AL4V/INCONEL 625 dissimilar welded joints. Ocean Eng. 221, 108582.
Cui, W.C., 2013. Development of the jiaolong deep manned submersible. Mar. Technol. Soc. J. 47, 37–54.
Dai, Q., Zhou, C.Y., Peng, J., He, X.H., 2015. Room-temperature creep behavior on crack tip of commercially pure titanium. Mater. Des. 85, 618–625.
Dong, C.L., Yu, H.C., Jiao, Z.H., Kong, F.T., Chen, Y.Y., 2018. Low cycle fatigue, creep and creep-fatigue interaction behavior of a TiAl alloy at high temperatures. Scripta Mater. 144, 60–63.

Gray, V., Whittaker, M., 2015. Development and assessment of a new empirical model for predicting full creep curves. J. Mater. 8, 4582–4592.
Gudipati, P.P., Kosaka, Y., 2011. Creep behavior of high temperature titanium alloys at low stress-high temperature regime. In: Proceedings of 12th World Conference on Titanium (Ti-2011), pp. 1227–1230.
Harrison, W.J., Whittaker, M.T., Lancaster, R.J., 2013. A model for time dependent strain accumulation and damage at low temperatures in Ti–6Al–4V. Mater. Sci. Eng., A 574, 130–136.
Jaworski, A.W., Ankem, S., 2006. Influence of the second phase on the room-temperature tensile and creep deformation mechanisms of alpha-beta titanium alloys. Metall. Mater. Trans. A 37, 2755–2765.
Kassner, M.E., Smith, K.K., 2014. Low temperature creep plasticity. J. Mater. Res. Technol. 3, 280–288.
Kassner, M.E., Smith, K.K., Campbell, C.S., 2015. Low temperature creep in pure metals and alloys. J. Mater. Sci. 50, 6539–6551.
Kotkunde, N., Deole, A.D., Gupta, A.K., Singh, S.K., 2014. Comparative study of constitutive modeling for Ti–6Al–4V alloy at low strain rates and elevated temperatures. Mater. Des. 55, 999–1005.
Kumar, J., Rao, A.V., Raman, S.G., Kumar, V., 2018. Creep-fatigue damage simulation at multiple length scales for an aeroengine titanium alloy. Int. J. Fatig. 116, 505–512.
Lamé, M.G., 1852. Leçons sur la théorie mathématique de l'elasticité des corps solides. Paris, France, Bachelier.
Ma, L.X., Wan, M., Li, W.D., Shao, J., Bai, X.P., Zhang, J.C., 2021. Superplastic deformation mechanical behavior and constitutive modelling of a near-α titanium alloy TNW700 sheet. Mater. Sci. Eng., A 817, 141419.
Neeraj, T., Hou, D.H., Daehn, G.S., Mills, M.J., 2000. Phenomenological and microstructural analysis of room temperature creep in titanium alloys. Acta Mater. 48, 1225–1238.
Pan, B.B., Cui, W.C., 2010. An overview of buckling and ultimate strength of spherical pressure hull under external pressure. Mar. Struct. 23, 227–240.
Pan, B.B., Cui, W.C., 2012. Structural optimization for a spherical pressure hull of a deep manned submersible based on an appropriate design standard. J. Ocean. Eng. 37, 564–571.
Peng, J., Zhou, C.Y., Dai, Q., He, X.H., 2014. The temperature and stress dependent primary creep of CP-Ti at low and intermediate temperature. Mater. Sci. Eng., A 611, 123–135.
Sato, E., Yamada, T., Tanaka, H., Jimbo, I., 2006. Categorization of ambient-temperature creep behavior of metals and alloys on their crystallographic structures. Mater. Trans. 47, 1121–1126.
Savage, M.F., Neeraj, T., Mills, M.J., 2002. Observations of room temperature creep recovery in titanium alloys. Metall. Mater. Trans. A 33, 891–898.
Sun, C.Q., Li, Y.Q., Huang, R.X., Wang, L., Liu, J.L., Zhou, L.L., Duan, G.H., 2020. Crack initiation mechanism and fatigue life of titanium alloy Ti–6Al–2Sn–2Zr–3Mo-X: effects of stress ratio and loading frequency. Mater. Sci. Eng., A 798, 140265.
Takagawa, T., Momma, H., Hotta, H., 1995. Advanced technology used in Shinkai 6500 and full ocean depth ROV Kaiko. Mar. Technol. Soc. J. 29, 15–25.
Wang, F., Cui, W.C., 2015. Experimental investigation on dwell-fatigue property of Ti-6Al-4V ELI used in deep-sea manned cabin. Mater. Sci. Eng., A 642, 136–141.
Wang, K., Wu, L., Li, Y.Z., Sun, X.P., 2020. Study on the overload and dwell-fatigue property of titanium alloy in manned deep submersible. China Ocean Eng. 34, 738–745.
Wang, L., Qu, P., Li, Y.Q., Huang, J.H., Wan, Z.Q., 2018. Theoretical and experimental investigations for creep properties of titanium alloy materials. J. Ship Mech. 22, 464–474 ([in Chinese]).
Xi, G.K., Lei, J.F., Qiu, J.K., Ma, Y.J., Yang, R., 2020. A semi-quantitative explanation of the cold dwell effect in titanium alloys. Mater. Des. 194, 108909.
Yang, X.J., Ling, X., 2017. Application of a composite model in the analysis of creep deformation at low and intermediate temperatures. J. Eng. Mater. Technol. 139, 041013.
Yu, C.L., Guo, Q.B., Gong, X.B., Yang, Y.F., Zhang, J., 2022. Fatigue life assessment of pressure hull of deep-sea submergence vehicle. Ocean Eng. 245, 110528.
Yu, W.X., Hou, S.S., Yang, Z.J., Zhang, J.Y., Lang, S.T., 2020. Characterization and modeling of room-temperature compressive creep behavior of a near TA31 titanium alloy. Metals 10, 1190.
Zhang, J., Zhang, M., Cui, W.C., Tang, W.X., Wang, F., Pan, B.B., 2018. Elastic-plastic buckling of deep sea spherical pressure hulls. Mar. Struct. 57, 38–51.
Zhang, M.Y., Gu, B.Q., Tao, J.H., 2018. Influence of sequential room-temperature compressive creep on flow stress of TA2. Mater. Res. Express 5, 36510.